Available online at www.sciencedirect.com

ScienceDirect

Ceramics International 40 (2014) 1605–1611

CERAMICS INTERNATIONAL

www.elsevier.com/locate/ceramint

Spectroscopic and structural features of Eu^{3+}-doped zinc pyrophosphate ceramic

Lin Qin[a], Chuanyan Xu[a], Yanlin Huang[a,*], Sun Il Kim[b], Hyo Jin Seo[b,*]

[a]College of Chemistry, Chemical Engineering and Materials Science, Soochow University, Suzhou 215123, China
[b]Department of Physics and Interdisciplinary Program of Biomedical Engineering, Pukyong National University, Busan 608-737, Republic of Korea

Received 21 June 2013; received in revised form 10 July 2013; accepted 10 July 2013
Available online 17 July 2013

Abstract

Eu^{3+}-doped pyrophosphate ceramic $SrZnP_2O_7$ was prepared by the solid-state reaction method. The ceramic was investigated by XRD, SEM, photoluminescence excitation and emission spectra, and decay curves. The red luminescence only arises from the $^5D_0$ level of Eu^{3+} ions. The microstructure was investigated by the luminescence probe of Eu^{3+} ion. There are two kinds of Eu^{3+} luminescence centers, which occupy both Sr^{2+} and Zn^{2+} sites. The energy transfers could only be detected from the Eu^{3+} ions doped on Zn^{2+}-sites to those on Sr^{2+}-sites. The possible defects and charge compensation mechanisms were discussed on the base of crystal structure and luminescence properties. Besides, the reason why the luminescence of Eu^{3+} doped on Zn^{2+}-sites is quenched at room-temperature was analyzed.

Keywords: A. Optical ceramics; B. Crystallization; C. Fluorescence

1. Introduction

Compounds doped with rare-earth ions (RE) are important functional materials for optical technology and luminescence display due to the rich $4f$–$4f$ transitions in $4f^n$ ions [1–6]. Phosphate has been paid great attentions because of its excellent properties, e.g., large band gap and high absorption in VUV–UV region, the moderate phonon energy, high chemical stability and exceptional optical damage threshold [7,8].

The crystal structures of pyrophosphates $M_2P_2O_7$ and $(A, M)_2P_2O_7$ (A and/or M an alkaline earth or divalent 3d-metal ion) have been widely investigated in the past decades [9–12]. Different applications of pyrophosphates have been reported, for example, the photoluminescence of RE-doped $Sr_2P_2O_7$ [13] and α-$Ca_2P_2O_7$ [14], magnetic properties of $BaMP_2O_7$ [15], $FePb_{1-x}Ba_xP_2O_7$ ($0 \le x < 1$) [16], and AMP_2O_7 (A = Mg, Ca, Sr or Ba; M = Cr, Mn, Co, Ni, Cu, Zn, Cd or Pb) [17], dielectric properties of $SrZnP_2O_7$ composites [18], etc.

Mixed pyrophosphates $SrMP_2O_7$ (M = Mg, Ca, Ba, Zn, Cr, Mn, Fe, Co, Ni, Cu, Cr or Cd) can form a series of compounds, which are all isostructural to α-$Ca_2P_2O_7$. There are two cation positions in α-$Ca_2P_2O_7$, i.e Ca(1) and Ca(2). They correspond to the Sr^{2+} and M in $SrMP_2O_7$ structure. The difference is that the coordination number of M sites in $SrMP_2O_7$ decreases from 8 in α-$Ca_2P_2O_7$ to 5, leading to the $[MO_5]$ groups [11,19]. For example, $SrZnP_2O_7$ belongs to the series of isotypic crystal structures and is closely related to α-$Ca_2P_2O_7$. Fig. 1(a) is a projection, on to [100], showing the distribution of ions in $SrZnP_2O_7$ structure. The unit contains two independent phosphorus centers tetrahedrally coordinated; Zn^{2+} shows a (4+1) square-pyramidal coordinated with oxygen. ZnO_5 and P_2O_7 build a three-dimensional framework with channels; Sr ions occupy the channels surrounded by eight O atoms. The spatiality of this structure is the chain arrangements of SrO_8 dodecahedron along the [010] direction as shown in Fig. 1(b).

Luminescence properties of RE-doped $SrZnP_2O_7$ have been paid great attentions. Höppe et al. [20] investigated the structure and luminescence of $SrMP_2O_7$ (M = Zn, Sr) co-actived with Eu^{2+} and Mn^{2+}. It is suggested that for the co-doping of Eu^{2+} and Mn^{2+} in $SrZnP_2O_7$, it is desirable to keep the Sr–Zn distance as short as possible for the energy-transfer from Eu^{2+} to Mn^{2+}, because

*Corresponding authors. Tel.: +82 51 629 5568; fax: +82 51 629 5549.
E-mail addresses: huang@suda.edu.cn (Y. Huang), hjseo@pknu.ac.kr (H.J. Seo).

0272-8842/$ - see front matter © 2013 Elsevier Ltd and Techna Group S.r.l. All rights reserved
http://dx.doi.org/10.1016/j.ceramint.2013.07.049

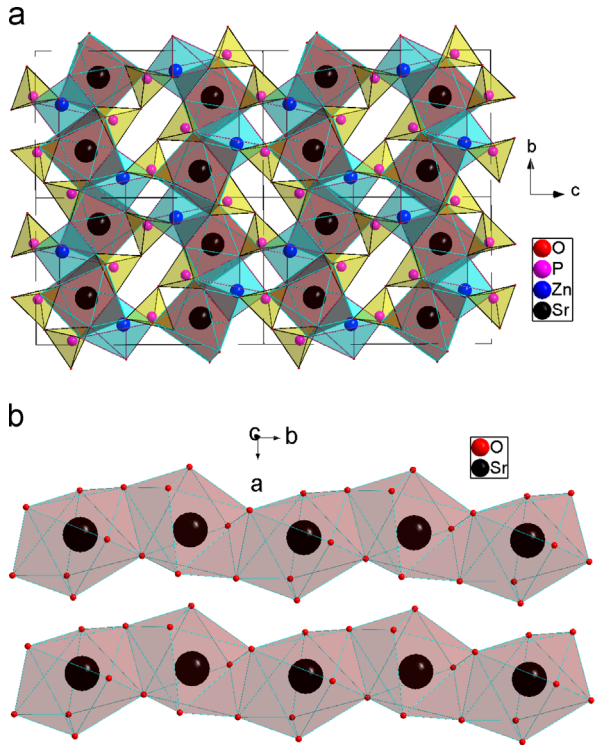

Fig. 1. (a) The schematic views of double unit cell of $SrZnP_2O_7$ structure along *a*-direction and (b) the coordination geometries of SrO_8 chains along *b*-direction.

ZnO_5 and SrO_8 are directly connected via a common O bridge. Yuan et al. [21] reported that the quantum efficiency of violet–blue emitting phosphor $SrZnP_2O_7$:Eu^{2+} was as high as 96% of the standard commercial $BaMgAl_{10}O_{17}$:Eu^{2+} phosphor. as a phosphor, $SrZnP_2O_7$:Eu^{2+} exhibits great potentials such as ultraviolet light emitting diode and photo-therapy lamps. Besides the efficient energy transfer from Eu^{2+} to Mn^{2+} [22], and Ce^{3+} to Tb^{3+} [23] take place in $SrZnP_2O_7$ host.

In this work, we gave a deep investigation to answer the question where the RE ions can be accommodated in pyrophosphate lattices. There are two cations (Sr and Zn) in the $SrZnP_2O_7$ host, it is a question where or which site between Sr and Zn the RE ions will occupy in this lattice. Eu^{3+} is selected as the structural probe to investigate the crystallographic distribution and the microstructure environments of Eu^{3+} ions in $SrZnP_2O_7$ ceramics.

2. Experimental

Eu^{3+}-doped $SrZnP_2O_7$ ceramics were prepared by the solid-state reaction method using stoichiometric amounts of high purity fine powders: $SrCO_3$, ZnO, $NH_4H_2PO_4$ and Eu_2O_3. Firstly, the mixture was ball-milled for 2 h with water. The slurry was dried and pre-heated at 850 °C for 6 h. Then calcined powders were ball-milled again with water and some organic dispersant. The mixture was dried again and uniaxially pressed into pellets. The pellet was sintered at 1000 °C for 6 h in air atmosphere.

The X-ray diffraction (XRD) patterns were collected on a Rigaku D/Max-2000 diffractometer operating at 40 kV, 30 mA with Bragg–Brentano geometry by using Cu Kα radiation ($\lambda = 1.5418$ Å). The optical excitation and emission spectra were recorded by a Perkin-Elmer LS-50B luminescence spectrometer and a Hitachi F-4500 fluorescence spectrophotometer.

The excitation source is a dye laser (Spectron Laser Sys. SL4000) pumped by the second harmonic (532 nm) of a pulsed Nd:YAG laser (Spectron Laser Sys. SL802G). The samples were placed in a liquid helium flow cryostat for measurements in the variable-temperature region (15–300 K). The laser beam was focused inside the sample with a cross-sectional area of about 3 mm^2. The 355 nm pulsed laser with about 7 mJ pulse energy was used for UV-irradiation on the samples. The luminescence decays were measured by monitoring the given emission from the samples under the pulsed laser excitation. The luminescence was dispersed by a 75 cm monochromator (Acton Research Corp. Pro-750) and observed with a photomultiplier tube (PMT) (Hamamatsu R928). Suitable filters were used to eliminate the intense laser scattering. The slit widths of the monochromator were normally set to give a resolution of 0.025 nm for emission spectra and the pulse width of 5 ns. Decay profiles were recorded with a LeCloy 9301 digital storage oscilloscope in which the signal was fed from PMT, and were fitted to appropriate one- or two-exponential functions to obtain the lifetimes of emitting levels.

3. Results and discussions

3.1. The phase formation

Fig. 2 shows the X-ray powder diffraction patterns of 0.5 mol% Eu^{3+}-doped $SrZnP_2O_7$ compared with the PDF2 card number 49-1026 ($SrZnP_2O_7$) selected from the International Centre for Diffraction Data (ICDD) database. It is clear that the positions and relative intensities of the main peaks in the samples match well with the standard card. No impurity

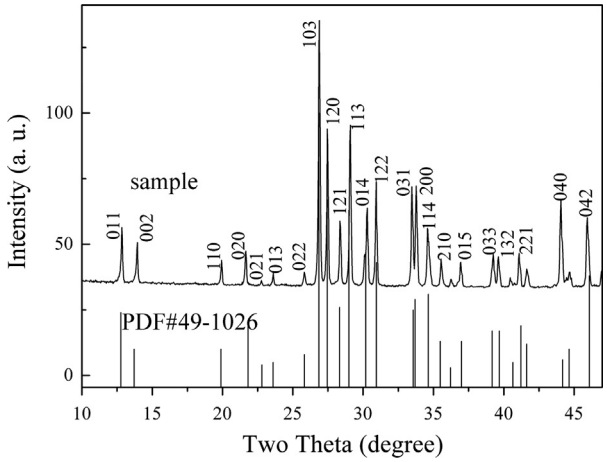

Fig. 2. XRD pattern of Eu^{3+}-doped $SrZnP_2O_7$ compared with the corresponding standard PDF2 cards 49-1026.

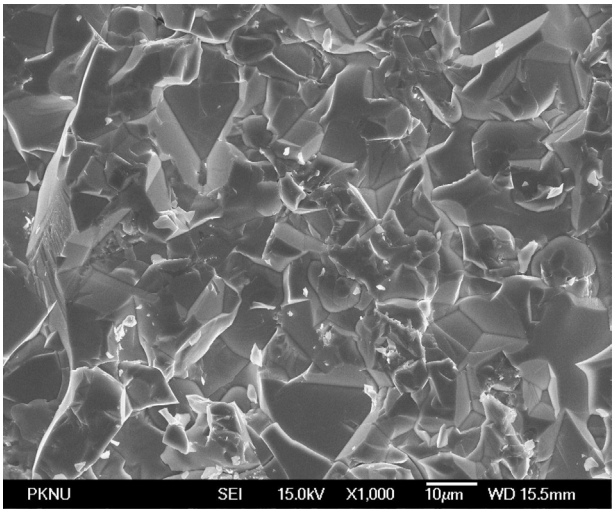

Fig. 3. The typical SEM image of Eu^{3+}-doped $SrZnP_2O_7$.

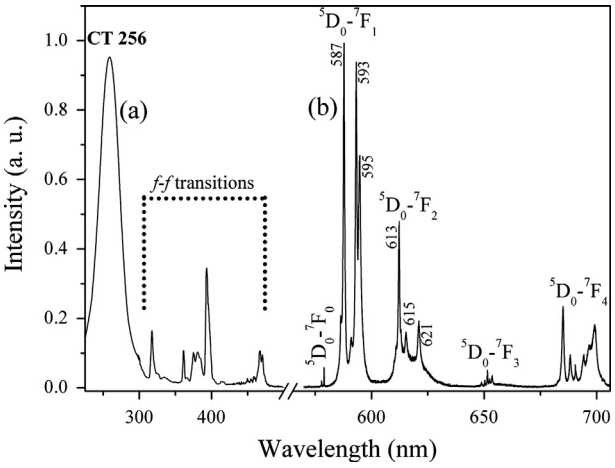

Fig. 4. The photoluminescence excitation (a: $\lambda_{em}=587$ nm) and emission (b: $\lambda_{ex}=254$) spectra of $SrZnP_2O_7$:Eu^{3+} 5 mol%.

lines were observed, and all the reflections could be well indexed to the $SrZnP_2O_7$ single phase.

Fig. 3 shows the SEM micrograph of $SrZnP_2O_7$ ceramic. The ceramic consists of closely packed grains. Furthermore, surfaces of the crystal grains are smooth, indicating that well-crystallized phosphate ceramics could be obtained under an air atmosphere.

3.2. Photoluminescence excitation and emission spectra

The photoluminescence excitation and emission spectra of $SrZnP_2O_7$:Eu^{3+} 5.0 mol % are shown in Fig. 4. The broad band in the excitation spectrum (Fig. 4a) from 200 to 300 nm with a maximum at 256 nm is the charge transfer (CT) from the 2*p* orbital of the O^{2-} to the 4*f* orbital of Eu^{3+} ions. The sharp lines in the region of 350–500 nm are transitions between the $^7F_0$ and $^5H_4$, $^5D_4$, ^5G_J, $^5L_6$, $^5D_{2,1}$ levels. Obviously, the intensity of the CT band is much stronger than that of *f*–*f* transitions in near UV wavelength. This indicates that the phosphors cannot be efficiently excited by the radiation of near UV-emitting InGaN based LED chips (around 400 nm).

Voort et al. [24,25] have investigated the influence of an effective charge at the Eu^{3+} ions on the quantum efficiency under charge-transfer (CT) excitation (q_{CT}) in the calcium and zirconium compounds. The results have been explained by a model which relates the sign of the effective charge to the shape and position of the parabola in the configurational coordinate diagram [24]. It has been suggested that the ions with intraionic transitions (*f*–*f* in Eu^{3+}) in some calcium compounds seem to show efficient luminescence if they have a positive effective charge. Whereas the luminescence of the ions are involved in an interionic transition (CT between Eu^{3+} and O^{2-}) is weak. A positive effective charge gave rise to a large relaxation in the CT state and a low q_{CT} value [26]. For a negative effective charge, the relaxation was predicted to be less and q_{CT} was high [24,27]. Followed by this model, it could be suggested that the effective positive charge of the Eu^{3+} ions at Sr^{2+} sites in $SrZnP_2O_7$ may be relatively weak.

The emission transitions of $^5D_0 \rightarrow {}^7F_{0,1,2,3,4}$ are convenient to characterize the different kinds of Eu^{3+} sites in a structure. Fig. 4(b) presents the emission spectrum of $SrZnP_2O_7$:$0.05Eu^{3+}$ excited by 254 nm (Hg lamp). The excitation of 254 nm can be considered as a non-selective one, all Eu^{3+} sites will be excited. There are groups of sharp lines assigned to the transitions of $^5D_0 \rightarrow {}^7F_J$ ($J=0$–4) levels of Eu^{3+}. The emission at about 580 and 613 nm are the transitions of $^5D_0 \rightarrow {}^7F_0$ and $^5D_0 \rightarrow {}^7F_2$, respectively. The emission intensities corresponding to the $^5D_0 \rightarrow {}^7F_{3,4}$ transitions are weak. The dominated red emission transitions of 587, 593, and 595 nm are attributed to the magnetic dipole transition of $^5D_0 \rightarrow {}^7F_1$, indicating that Eu^{3+} is located at the site of inversion symmetry [28].

Fig. 5 is the emission spectra in the region of $^5D_0 \rightarrow {}^7F_0$ transition under the excitation of 254 nm for the samples doped with Eu^{3+} of 0.5, 3.0 and 5.0 mol %. All the spectra show similar emission positions. Two emission peaks at 579.18 nm (17,266 cm^{-1}) and 578.06 nm (17,300 cm^{-1}) could be observed, which were labeled as *A* and *B*, respectively. Because there are no

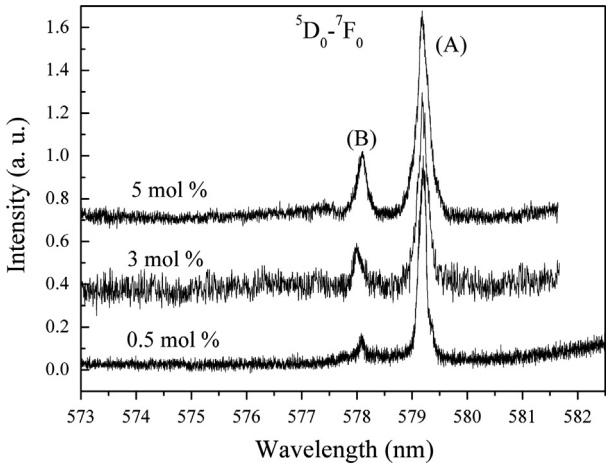

Fig. 5. The luminescence spectra of $SrZnP_2O_7$:Eu^{3+} 0.5, 3.0 and 5.0 mol% in the wavelength region of the $^5D_0 \rightarrow {}^7F_0$ transitions under excitation of 254 nm-UV light at 300 K.

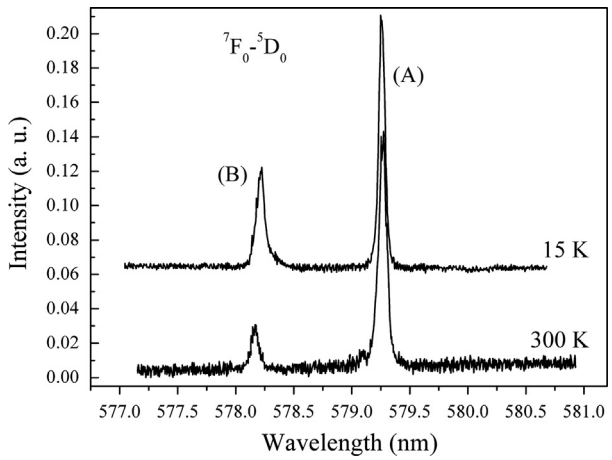

Fig. 6. The excitation spectra for $^7F_0 \rightarrow {}^5D_0$ transition of Eu^{3+} ions in $SrZnP_2O_7$:Eu^{3+} 0.5 mol%. The spectra were obtained by monitoring the total luminescence at 15 K and at 300 K. The spectra were obtained with a 580 nm filter before the sample and by setting monochrometer in zero order of diffraction to pass all the $^5D_0 \rightarrow {}^7F_J$ (J=0–4) emission of Eu^{3+} from the samples. The peaks are labeled by $Eu^{3+}(A)$ and $Eu^{3+}(B)$.

emissions from the upper energy level ($^5D_{1,2,}$) as mentioned above, the presence of two-site distributions in the $^5D_0 \rightarrow {}^7F_0$ transition range confirms that Eu^{3+} ions were introduced into the lattices on two different crystallographic sites.

3.3. The excitation spectra of $^7F_0 \rightarrow {}^5D_0$ transition

In order to confirm the two Eu^{3+} site-distributions, the excitation spectra of $SrZnP_2O_7$:0.05Eu^{3+} were investigated by monitoring the total luminescence using dye laser (Fig. 6). At 15 K and 300 K, only two excitation peaks at 579.18 nm $Eu^{3+}(A)$ and at 578.06 nm $Eu^{3+}(B)$ corresponding to $^7F_0 \rightarrow {}^5D_0$ transitions can be observed. The excitation site $Eu^{3+}(B)$ is weak, however, the site $Eu^{3+}(A)$ has a stronger intensity. This confirms that $Eu^{3+}(A)$ is the dominated site. The $^7F_0$ and $^5D_0$ levels are non-degenerant and the spectra associated with transitions between them should contain as many lines as the number of non-equivalent sites. This further indicates that Eu^{3+} ions occupy two sites in $SrZnP_2O_7$:Eu^{3+}.

3.4. The site-selective emission spectra

The site-selective emission spectra were recorded for $SrZnP_2O_7$:0.005Eu^{3+} under excitation into $Eu^{3+}(A)$ (Fig. 7a) at 300 K and $Eu^{3+}(B)$ sites (Fig. 7b) at 15 K. The results representing $^5D_0 \rightarrow {}^7F_J$ (J=1–4) emission clearly show two distinct spectra for two samples, especially in the case of $^5D_0 \rightarrow {}^7F_1$ transitions.

It is a well-known theory that the maximum splittings transitions for $^5D_0 \rightarrow {}^7F_J$ (J=0, 1, and 2) are 1, 3 and 5, respectively, for each site in a crystal field. In fact, under the selective excitation into the $^5D_0$ $Eu^{3+}(B)$, the emission spectrum (ex=578.06 nm) (Fig. 7b) presents more than 7 emission lines for that in $^5D_0 \rightarrow {}^7F_2$ transitions.

Two of the emission lines are located at the same position with those obtained under the selective excitation into $Eu^{3+}(A)$

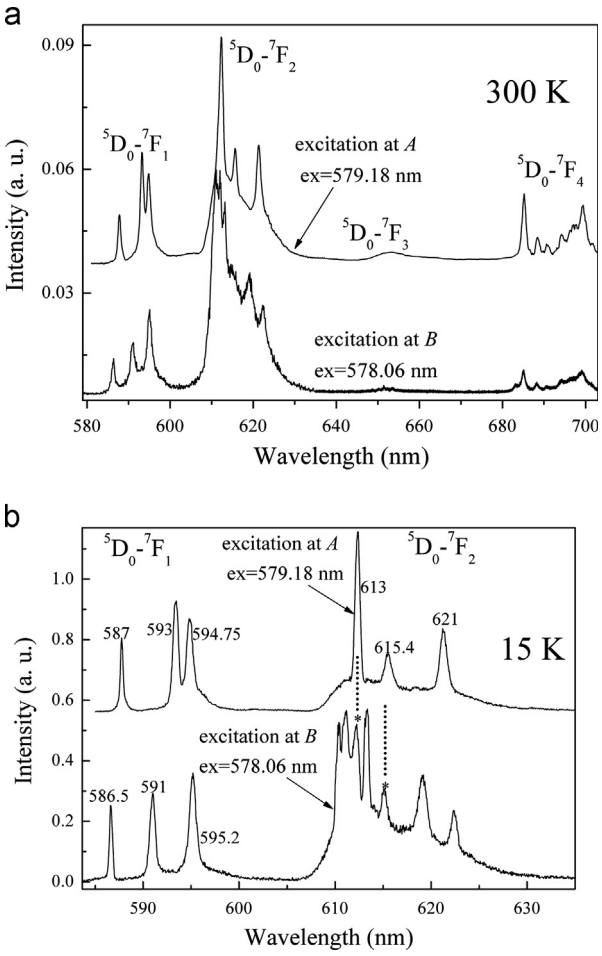

Fig. 7. The site-selective emission spectra of $^5D_0 \rightarrow {}^7F_J$ (J=1, 2) for the site $Eu^{3+}(A)$ exciting at 579.18 nm and that for $Eu^{3+}(B)$ at 578.06 nm at 300 K (a) and 15 K (b) in $SrZnP_2O_7$:Eu^{3+} 0.5 mol%. The symbols "*" labeled in Fig. (b) indicate the emission lines which are from Eu^{3+} site A.

(labeled as "*" in Fig. 7(b)). So under the excitation into $Eu^{3+}(B)$, the emission lines come from both $Eu^{3+}(A)$ and $Eu^{3+}(B)$ sites. In this case, by comparing the two spectra, the Stark components of the $^5D_0 \rightarrow {}^7F_J$ (J=0–2) transitions for the two sites can be derived and are reported in Table 1. The fact that the emission from $Eu^{3+}(A)$ can be observed under the site-selective into $Eu^{3+}(B)$ means the energy transfer occurs from $Eu^{3+}(B)$ (higher energy site) to $Eu^{3+}(A)$ (lower energy site), and the energy transfer from $Eu^{3+}(A)$ to $Eu^{3+}(B)$ cannot occur.

In order to confirm this kind of energy transfer between the two Eu^{3+} sites, the site-selective excitation spectra were measured by singly monitoring emission from $^5D_0 \rightarrow {}^7F_1$ transition of $Eu^{3+}(A)$ (at 587 nm) and $^5D_0 \rightarrow {}^7F_1$ transition (591 nm) of $Eu^{3+}(B)$, respectively (see Fig. 8(a)). The excitation spectrum by monitoring the $Eu^{3+}(A)$ emission at 587 nm indicates that the excitation comes from both $Eu^{3+}(A)$ and $Eu^{3+}(B)$. However, the excitation spectrum of $Eu^{3+}(B)$-emission at 591 nm shows the excitation line only comes from site B itself (Fig. 8(b)). This indicates the existence of the energy transfer from $Eu^{3+}(B)$ to $Eu^{3+}(A)$.

To further testify the energy transfer process, the fluorescence decay curves were measured. Fig. 9 shows the decay curves of

Table 1
The wavelength (nm and cm^{-1}) and energy assignments of $^5D_0 \rightarrow {}^7F_J$ ($J=0$–2) transitions for $SrZnP_2O_7:Eu^{3+}$.

	$Eu^{3+}(A)$		$Eu^{3+}(B)$	
	nm	cm^{-1}	nm	cm^{-1}
$^5D_0 \rightarrow {}^7F_0$	579.18	17,266	578.06	17,300
$^5D_0 \rightarrow {}^7F_1$	587	17,035	586.5	17,051
	593	16,863	591	16,920
	594.75	16,814	595.7	16,786
$^5D_0 \rightarrow {}^7F_2$	613	16,313	610.5	16,380
	615.4	16,250	611.1	16,364
	621	16,103	613.6	16,297
			619.2	16,150
			622.3	16,070
$\Delta E(^7F_1)$		221		265

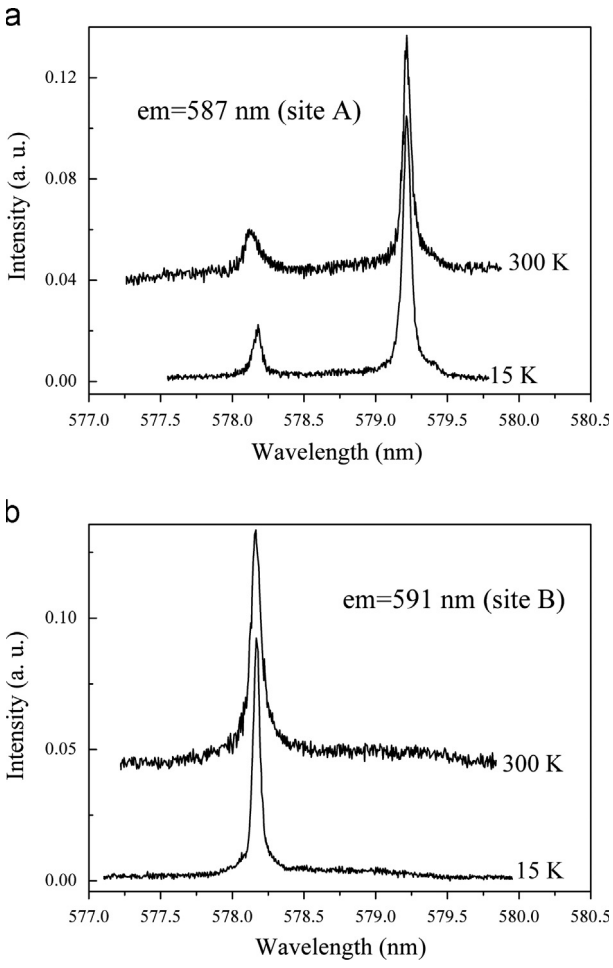

Fig. 8. (a) The site-selective excitation spectra by monitoring $^5D_0 \rightarrow {}^7F_1$ emission (587 nm in Fig. 7(b) from $Eu^{3+}(A)$ and (b) by monitoring $^5D_0 \rightarrow {}^7F_1$ emission (591 nm in from $Eu^{3+}(B)$ at 300 K and 10 K.

$^5D_0 \rightarrow {}^7F_1$ emission under excitation in $Eu^{3+}(A)$ and $Eu^{3+}(B)$ sites at 300 K. The luminescence from $Eu^{3+}(A)$ exhibits an exponential decay with a lifetime constant 1.85 μs (Fig. 9). However, $^5D_0 \rightarrow {}^7F_1$ from $Eu^{3+}(B)$ displays a non-exponential decay with the average lifetime of 0.81 μs (Fig. 9). Such an

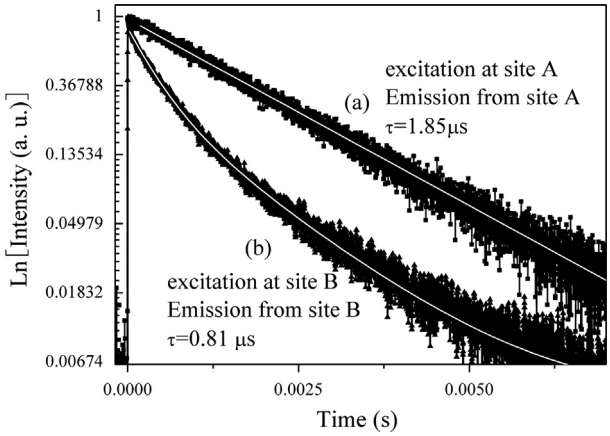

Fig. 9. The $^5D_0 \rightarrow {}^7F_1$ luminescence decay curves under the excitation of $Eu^{3+}(A)$ and that of $Eu^{3+}(B)$ by monitoring $^5D_0 \rightarrow {}^7F_1$ emission in Fig. 7(b) from $Eu^{3+}(A)$ and $Eu^{3+}(B)$.

observation indicates a possible site-to-site energy transfer, $Eu^{3+}(B)$ is the energy donor and $Eu^{3+}(A)$ is the energy acceptor.

Usually, the luminescence from an isolated ion shows an exponential decay with a certain lifetime τ [29]. When any energy transfer occurs from a donor to an acceptor, the decay of the donor emitting ions could be non-exponential depending on average donor–acceptor distance. The non-exponential decay curve in Fig. 9(b) can be fitted to the energy transfer model suggested by Inokuti and Hirayama [30]. The energy transfer process for the dipole–dipole interaction between two Eu^{3+} ions is given by the equation

$$I(t) = I_0 \exp\left[-\frac{t}{\tau_0} - \alpha\left(\frac{t}{\tau_0}\right)^{1/2}\right] \quad (1)$$

where, I_0 is the initial emission intensity for $t=0$, τ_0 is intrinsic lifetime of donor ions, and α is a constant which includes energy transfer rate and critical energy transfer distance (R_0) of donor–acceptor depending on temperature [30]. The intrinsic lifetime for $Eu^{3+}(B)$ site obtained by fitting the decay from Eq. (1) is 1.24 ms (τ_0).

It is expected that the emission from $Eu^{3+}(A)$, e.g. the lines indicated by "✻" in Fig. 7(b), has a rise time in the initial stage by exciting $Eu^{3+}(B)$ because the energy transfer process leads to feeding the $^5D_0$ state of $Eu^{3+}(A)$. However, no clear buildup of the $^5D_0$ state for $Eu^{3+}(A)$ was observed in the decay.

3.5. The structural assignments of Eu^{3+} ions

$SrZnP_2O_7$ crystallizes in a monoclinic system with the space group of $P2_1/n$ (14). The unit cell has four crystallographically independent cation sites, i.e., one Sr^{2+} site (Wyckoff 4*e* site) with coordination number (CN) of 8, one five-coordinated Zn^{2+} site and two four-coordinated P^{5+} sites. The [ZnO_5] units and the [P_2O_7] groups form a three-dimensional framework with channels along [100] and [010], in which the Sr^{2+} ions fill [20,31]. However, two sites were identified for Eu^{3+} ions in the $SrZnP_2O_7$

lattice, that is, $Eu^{3+}(A)$ at 579.18 nm and $Eu^{3+}(B)$ at 578.06 nm by site-selective laser-excitation spectroscopy.

The possible defects could be generated in the hosts as Eu^{3+} ions were doped in $SrZnP_2O_7$ lattices because of 2+ valences of cations Sr^{2+} and Zn^{2+}, it could be proposed that Eu^{3+} ions will occupy Sr^{2+} or Zn^{2+} sites. The charge compensation can be achieved by two possible mechanisms: the first is that Eu^{3+} ions substitute for Sr^{2+} or Zn^{2+} and combine with Sr^{2+} or Zn^{2+} vacancies, this forms a dipole complex of $[2(Eu_{Sr}^{3+})^{\bullet}\text{-}V''_{Sr}]$ or $[2(Eu_{Zn}^{3+})^{\bullet}\text{-}V''_{Zn}]$. This is a very common mechanism in RE doped inorganic components such as Eu^{3+}-doped apatites [32]; and the second mechanism is related to interstitial oxygen, O_i, in the lattices $[2(Eu_{Sr}^{3+})^{\bullet}\text{-}O''_i]$ or $[2(Eu_{Zn}^{3+})^{\bullet}\text{-}O''_i]$.

The ionic radii of Eu^{3+} (CN=8), Sr^{2+} (CN=8) and Zn^{2+} (CN=5) are 1.066 Å, 1.26 Å, and 0.66 Å, respectively, then Eu^{3+} ions occupy preferably Sr^{2+} sites. So the dominated $Eu^{3+}(A)$ could be assigned to Eu^{3+} ions occupying on Sr^{2+} sites in the lattices. It can be seen from the emission spectra in Fig. 5 that $^5D_0 \rightarrow {}^7F_0$ emission at *A* 579.18 nm (17,266 cm^{-1}) is dominated at any Eu^{3+} doping level. This is reasonable that Eu^{3+} ions prefer to occupy Sr^{2+} site over Zn^{2+} site. The remained $Eu^{3+}(B)$ site could be assigned to Eu^{3+} occupying on Zn^{2+} sites on the base of the luminescence results by the following facts.

Firstly, $Eu^{3+}(A)$ presents longer luminescence decay lifetime than that of $Eu^{3+}(B)$. Usually, Eu^{3+} centers with shorter lifetime are correlated to a more flexible Eu^{3+}-local structure, whereas the ones with longer lifetime corresponds to more rigid ligands-to-metal local surroundings [33]. In $SrZnP_2O_7$ lattices, Zn^{2+} ions occupy square-pyramidal coordination and are isolated in the structure. However, the edge-shared SrO_8 form zig-zag chains along [010] direction in interlayer between $[ZnO_5]$ units and $[P_2O_7]$ groups [20]. The surroundings of Sr^{2+} ions are more rigid than that of Zn^{2+} ions.

Secondly, the energy of $^5D_0 \rightarrow {}^7F_0$ transition could be related to the covalency degree of the Eu–O environments on the base of the nephelauxetic effect [34,35]. The maximum splitting of $^7F_1$ manifold, $\Delta E(^7F_1)$, is associated with the overall electrostatic energy of Eu^{3+} local environments [33]. The high-energy $^5D_0 \rightarrow {}^7F_0$ transition at 578.06 nm $Eu^{3+}(B)$ has high-field sites with $\Delta E(^7F_1)$ of 265 cm^{-1} (Table 1) indicating that Eu–O bonding is less covalent. Moreover, the low-energy $^5D_0 \rightarrow {}^7F_0$ transition at 579.18 nm $Eu^{3+}(A)$ represents low-field sites $\Delta E(^7F_1)=221$ cm^{-1}, where the Eu–O bondings are more covalent. This could be explained by the required charge compensations: $[2(Eu_{Zn}^{3+})^{\bullet}\text{-}V''_{Zn}]$ for the substitution of the Zn^{2+} ions by $Eu^{3+}(B)$, and $[2(Eu_{Sr}^{3+})^{\bullet}\text{-}O''_i]$ for $Eu^{3+}(A)$ on Sr^{2+} sites.

Thirdly, the complex of $[2(Eu_{Sr}^{3+})^{\bullet}\text{-}O_i'']$ mentioned above for $Eu^{3+}(A)$ on Sr^{2+} is possible. In $SrZnP_2O_7$, $[ZnO_5]$ units and the $[P_2O_7]$ groups construct pseudo-layered framework along [010], Sr^{2+} ions occupy cavities between two pseudo-layers (Fig. 1(a)). There are ample spaces to arrange O_i'' to compensate the defects due to the substitution of Eu^{3+} on Sr^{2+} sites. It is not difficult to create O_i'' due to material preparation in air atmosphere. This kind of mechanism is also confirmed in the other oxides, e.g., the RE-doped the apatite [36] and scheelite [37] structure materials.

Finally, similar occupations on both Sr^{2+} and Zn^{2+} sites have been reported for Mn^{2+} in $SrZnP_2O_7$. It has been concluded that Mn^{2+} ions located on Sr^{2+} sites emit at 640 nm while those positioned on Zn^{2+} site are responsible for the emission around 530 nm. Considering the ionic radii Eu^{3+} (1.066 Å) and Mn^{2+} (0.96 Å), it could be proposed that Eu^{3+} ions could occupy both Sr^{2+} and Zn^{2+} sites. However, Eu^{3+} ions will occupy preferably the Sr^{2+} site.

3.6. The quenching of one of Eu^{3+} ions:$Eu^{3+}(B)$

At room temperature, it seems that the fluorescence from site $Eu^{3+}(B)$ is greatly quenched. This could be found on the emission spectrum (254 nm excitation) in Fig. 4, where the emission lines have nearly the same position as those in Fig. 7. It has been reported that phonon-assisted energy transfer played an important role in the infrared-to-visible conversion process in the phosphors activated with RE ions [38]. In Eu^{3+}-doped $SrZnP_2O_7$, the energy transfer between $Eu^{3+}(A)$ and $Eu^{3+}(B)$ is a non-resonant process because of the energy mismatch of 34 cm^{-1} (Table 1). Therefore, the energy transfer requires the assistance of phonons, this phonon assistance causes the enhancement of energy transfer probability with increasing temperature. Consequently, $Eu^{3+}(B)$ site is quenched at high temperature.

4. Conclusions

According to the results of the laser site-selective excitation and emission spectroscopy for Eu^{3+} ions, it can be suggested that rare earth ions can be doped into two crystallographic sites in pyrophosphate lattices. In the case of Eu^{3+}-doped $SrZnP_2O_7$, the dominated site (*A* at 579.18 nm) is assigned to the $Eu^{3+}(A)$ ions occupying on the Sr^{2+} sites in the lattices by the charge compensation of $[2(Eu_{Sr}^{3+})^{\bullet}\text{-}O''_i]$, while another minor one $Eu^{3+}(B$: 578.06 nm) could be assigned to the Eu^{3+} ions occupying on the Zn^{2+} by the charge compensation of $[2(Eu_{Zn}^{3+})^{\bullet}\text{-}V''_{Zn}]$. The site-selective excitation and emission spectra together with the luminescence decays indicate that the energy transfer occurs from $Eu^{3+}(B)$ to $Eu^{3+}(A)$. However, no energy transfer can take place from $Eu^{3+}(A)$ to $Eu^{3+}(B)$. The $Eu^{3+}(A)$ center exhibits a predominant luminescence at RT. At room temperature, it seems that the fluorescence from site $Eu^{3+}(B)$ are quenched. The photoluminescence excitation and emission spectra of $SrZnP_2O_7$:Eu^{3+} show that the intensity of the CT band is much stronger than that of *f–f* transitions in the near UV wavelength. $SrZnP_2O_7$:Eu^{3+} can be efficiently excited by the UV light, but cannot be efficiently excited by the radiation of near UV-emitting InGaN based LED chips (around 400 nm).

Acknowledgments

This research was supported by Basic Science Research Program through the National Research Foundation of Korea (NRF) funded by the Ministry of Science, ICT & Future Planning (NRF-2013-R1A1A2009154) and by a Project Funded by the Priority Academic Program Development of Jiangsu Higher Education Institutions (PAPD).

References

[1] P. Huang, F. Yang, C. Cui, L. Wang, X. Lei, Luminescence improvement of $Y_2O_2S:Tb^{3+}$, Sr^{2+}, Zr^{4+} white-light long-lasting phosphor via Eu^{3+} addition, Ceramics International 39 (2013) 7193–7197.

[2] Z.P. Yang, Y.F. Liu, C. Liu, F. Yang, Q.M. Yu, X. Li, F.C. Lu, Multiwavelength excited white-emitting Dy^{3+} doped $Sr_3Bi(PO_4)_3$ phosphor, Ceramics International 39 (2013) 7279–7283.

[3] E. Pavitra, G.S.R. Raju, J.S. Yu, White light emission from Eu^{3+} co-activated $Ca_2Gd_8Si_6O_{26}:Dy^{3+}$ nanophosphors by solvothermalsynthesis, Ceramics International 39 (2013) 6319–6324.

[4] M. Kahlaoui, S. Chefi, A. Inoubli, A. Madani, C. Chefi, Synthesis and electrical properties of co-doping with La^{3+}, Nd^{3+}, Y^{3+}, and Eu^{3+} citric acid-nitrate prepared samarium-doped ceria ceramics, Ceramics International 39 (2013) 3873–3879.

[5] S.A. Hassanzadeh-Tabrizi, E. Taheri-Nassaj, Polyacrylamide gel synthesis and sintering of $Mg_2SiO_4:Eu^{3+}$ nanopowder, Ceramics International 39 (2013) 6313–6317.

[6] M. Erdem, G. Özen, C. Tav, B.D. Bartolo, Structural and spectroscopic properties of $Nd^{3+}:Y_2Si_2O_7$ phosphors, Ceramics International 39 (2013) 6029–6033.

[7] B.K. Grandhe, V.R. Bandi, K. Jang, Ho-Sueb Lee, Dong-Soo Shin, S.S. Yi, Jung-Hyun Jeong, Effect of sintering atmosphere and lithium ion co-doping on photoluminescence properties of $NaCaPO_4:Eu^{2+}$ phosphor, Ceramics International 38 (2012) 6273–6279.

[8] C.H. Moo, S.K. Singh, D.G. Lee, S.S. Yi, K. Jang, J.H. Jeong, J.S. Bae, D.S. Shin, Synthesis and optical characterization of novel $Sr_3Ga_2O_6:Eu^{3+}$ phosphor, Ceramics International 38 (2012) 6789–6794.

[9] C. Calvo, Crystal structure of alpha-calcium pyrophosphate, Inorganic Chemistry 7 (1968) 1345–1351.

[10] C. Calvo, Crystallographic character of the $Sr_{2-x}MgxP_2O_7$ system, Journal of the Electrochemical Society 115 (1968) 1095–1096.

[11] A.A. Tahiri, B. ElBali, M. Lachkar, R. Ouarsal, P.Y. Zavalij, $SrMgP_2O_7$, Acta Crystallographica E58 (2002) i9–i11.

[12] L.D. Hagmann, L. Jansson, C. Magneli, The crystal structure of alpha-$Sr_2P_2O_7$, Acta Chemica Scandinavica 22 (1968) 1419–1429.

[13] S. Ye, Z.S. Liu, J.G. Wang, X.P. Jing, Luminescent properties of $Sr_2P_2O_7$:Eu, Mn phosphor under near UV excitation, Materials Research Bulletin 43 (2008) 1057–1065.

[14] Z.D. Hao, J.H. Zhang, X. Zhang, X.Y. Sun, Y.S. Luo, S.Z. Lu, X. J. Wang, White light emitting diode by using α-$Ca_2P_2O_7:Eu^{2+}$, Mn^{2+} phosphor, Applied Physics Letters 90 (2007) 261113–261115.

[15] A.A. Belik, M. Azuma, M. Takano, Magnetic properties of isostructural $BaCoP_2O_7$, $BaNiP_2O_7$, and $BaCuP_2O_7$ studied with dc and ac magnetization and specific heat, Inorganic Chemistry 44 (2005) 7523–7529.

[16] O. Sqalli, B. Malaman, M. Ijjaali, Synthesis, crystal structure, and magnetic investigations of $FePb_{1-x}BaxP_2O_7$ ($0 \le x < 1$), Materials Letters 58 (2004) 2984–2987.

[17] A. Boukhari, A. Moquine, M. Flandrois, Synthesis and characterization of new copper (II) mixed diphosphates $(M,Cu)_2P_2O_7$ with M=Mg, Ca, Sr, and Ba, Journal of Solid State Chemistry 87 (1990) 251–256.

[18] H.T. Jiang, J.W. Zhai, X. Yao, Microwave dielectric properties of $BaTiO_3$–$SrZnP_2O_7$ composite ceramics for tunable microwave applications, Journal of Physics D: Applied Physics 42 (2009) 225404–225408.

[19] E.V. Murashova, Y.A. Velikodnyi, V.K. Trunov, Russian Journal of Inorganic Chemistry 36 (1991) 481–483.

[20] H.A. Höppe, M. Daub, M.C. Bröhmer, Coactivation of α-$Sr(PO_3)_2$ and $SrM(P_2O_7)$ (M=Zn, Sr) with Eu^{2+} and Mn^{2+}, Chemistry of Materials 19 (2007) 6358–6362.

[21] J.L. Yuan, X.Y. Zeng, J.T. Zhao, Z.J. Zhang, H.H. Chen, G.B. Zhang, Rietveld refinement and photoluminescent properties of a new blue-emitting material: Eu^{2+} activated $SrZnP_2O_7$, Journal of Solid State Chemistry 180 (2007) 3310–3316.

[22] Z.P. Yang, G.W. Yang, S.L. Wang, J. Tian, Q.L. Guo, G.S. Fu, Luminescence and energy transfer of Eu^{2+}, Mn^{2+} in $SrZnP_2O_7$, Chinese Physics Letters 24 (2007) 2094–2096.

[23] P. Li, H. Liu, Z. Wang, Z. Yang, X. Li, Y Yang, Luminescence and energy transfer of Ce^{3+}, Tb^{3+} in $SrZnP_2O_7$, Chinese Journal of Luminescence 5 (2010) 719–723.

[24] D.V.D. Voort, G. Blasse, Luminescence of the europium (3+) ion in zirconium (4+) compounds, Chemistry of Materials 3 (1991) 1041–1045.

[25] D.V.D. Voort, A. Imhof, G. Blasse, Quantum efficiencies of luminescent Eu^{3+} centers in CaO, Journal of Solid State Chemistry 96 (1992) 311–317.

[26] D.V.D. Voort, G. Blasse, Luminescence of $CaSO_4:Bi^{3+}$, a small-offset case, Journal of Solid State Chemistry 99 (1992) 404–408.

[27] D.V.D. Voort, J.M.E. de Rijk, R. van Doom, G. Blame, Luminescence of rare-earth ions in $Ca_3(BO_3)_2$, Materials Chemistry and Physics 31 (1992) 333–339.

[28] G. Blasse, B.C. Grabmaier, Luminescent Materials, Springer-Verlag, Berlin, 1994.

[29] R.K. Watts, H.J. Richter, Diffusion and transfer of optical excitation in YF_3:Yb, Ho, Physical Review B 6 (1972) 1584–1589.

[30] M. Inokuti, F. Hirayama, Influence of energy transfer by the exchange mechanism on donor luminescence, Journal of Chemical Physics 43 (1965) 1978–1989.

[31] M.V. Hoffman, Eu^{2+} activation in some alkaline earth strontium phosphate compounds, Journal of the Electrochemical Society 115 (1968) 560–563.

[32] M. Karbowiak, S. Hubert, Site-selective emission spectra of Eu^{3+}: $Ca_5(PO_4)_3F$, Journal of Alloys and Compounds 302 (2000) 87–93.

[33] J.P. Rainho, D. Ananias, Z. Lin, A. Ferreira, L.D. Carlos, J. Rocha, Photoluminescence and local structure of Eu(III)-doped zirconium silicates, Journal of Alloys and Compounds 374 (2004) 185–189.

[34] J.F.S. Menezes, O.L. Malta, Highly luminescent europium(III) complexes with naphtoiltrifluoroacetone and dimethyl sulphoxide, Molecular Physics 101 (2003) 1037–1045.

[35] C.K. Jørgensen, Progress in Inorganic Chemistry 4 (1962) 73–124.

[36] B. Piriou, D. Fahmi, J. Dexpert-Ghys, A. Taitai, J.L. Lacout, Unusual fluorescent properties of Eu^{3+} in oxyapatites, Journal of Luminescence 39 (1987) 97–103.

[37] Y.L. Huang, W.L. Zhu, X.Q. Feng, The effects of sequential annealing in air atmosphere on luminescence properties of $PbWO_4$ single crystal, Journal of Electron Spectroscopy and Related Phenomena 133 (2003) 39–45.

[38] M. Yamada, S. Shionoya, T. Kushida, Phonon-assisted energy transfer between trivalent rare earth ions, Journal of the Physical Society of Japan 32 (1972) 1577–1586.